

Hysteresis and bi-stability by an interplay of calcium oscillations and action potential firing

J.M.A.M. Kusters*, J.M. Cortes*,†‡, W.P.M. van Meerwijk§, D.L. Ypey§,
A.P.R. Thevenet§ and C.C.A.M. Gielen*

30th October 2018

* Dept. of Biophysics, Radboud University Nijmegen, Geert Grooteplein 21,
6525 EZ Nijmegen, The Netherlands

† Institute Carlos I for Theoretical and Computational Physics
and Departamento de Electromagnetismo y Fisica de la Materia.
Universidad de Granada, E-18071 Granada, Spain

‡ Institute for Adaptive and Neural Computation. School of Informatics,
University of Edinburgh, EH1 2QL, UK

§ Department of Cell Biology, Radboud University Nijmegen, Toernooiveld 1,
6525 ED Nijmegen, The Netherlands

Corresponding author: J.M.A.M. Kusters,
Dept. of Biophysics, Radboud University Nijmegen,
Geert Grooteplein 21, 6525 EZ Nijmegen, The Netherlands,
email: m.kusters@science.ru.nl, tel: +31-24-3615039, fax: +31-24-3541435

Abstract

Many cell types exhibit oscillatory activity, such as repetitive action potential firing due to the Hodgkin-Huxley dynamics of ion channels in the cell membrane or reveal intracellular inositol triphosphate (IP_3) mediated calcium oscillations (CaOs) by calcium-induced calcium release channels (IP_3 -receptor) in the membrane of the endoplasmic reticulum (ER). The dynamics of the excitable membrane and that of the IP_3 -mediated CaOs have been the subject of many studies. However, the interaction between the excitable cell membrane and IP_3 -mediated CaOs, which are coupled by cytosolic calcium which affects the dynamics of both, has not been studied. This study for the first time applied stability analysis to investigate the dynamic behavior of a model, which includes both an excitable membrane and an intracellular IP_3 -mediated calcium oscillator. Taking the IP_3 concentration as a control parameter, the model exhibits a novel rich spectrum of stable and unstable states with hysteresis. The four stable states of the model correspond in detail to previously reported growth-state dependent states of the membrane potential of normal rat kidney fibroblasts in cell culture. The hysteresis is most pronounced for experimentally observed parameter values of the model, suggesting a functional importance of hysteresis. This study shows that the four growth-dependent cell states may not reflect the behavior of cells that have differentiated into different cell types with different properties, but simply reflect four different states of a single cell type, that is characterized by a single model.

Key words: *Hysteresis; Bistability; Calcium Oscillations; Cell Signaling*

Complexity and multiple transitions among behavioral states are ubiquitous in biological systems (1, 2). In physics instabilities and hysteresis are well known to play an important role in collective properties and have been studied since many years (3, 4, 5, 6). Recently, multi-stability with hysteresis has also awakened a large interest in biological systems (7). Instabilities, for instance, are crucial for efficient information processing in the brain, such as in odor encoding (8, 9). Moreover, unstable dynamic attractors have been demonstrated in cortical networks, with critical relevance to working memory and attention (10, 11, 12). In a wide sense, multistable systems allow changes among different stable solutions where the system takes advantage of instabilities as gateways to switch between different stable branches (7). Bistability driven by instabilities prevents the system from reaching intermediate states, e.g. partial mitosis. Hysteresis prevents the system from changing its state when parameter values, that characterize the system, vary. This is of relevance, for instance, in cell mitosis. Once initiated, mitosis should not be terminated before completion (13). Thus, hysteresis may lock the cell into a fixed state, preventing it from sliding back to another state (14).

At the level of cell networks, multistability, and in particular bistability, plays an important role in cell signaling as well (15, 16). For example, communication between neurons takes place at synaptic contacts, where arrival of an action potential stimulates release of a neurotransmitter, thus affecting the post-synaptic potential of the target cell. Typically, each cell receives input from thousands of other cells mediated by different neurotransmitters, which modify the post-synaptic potential by excitation or inhibition at different time scales (17). This information at the cell membrane may be transferred to the cell nucleus by so-called second messengers to affect the nucleus in controlling DNA-expression, protein synthesis, mitosis, etc. Calcium is one such second messenger and calcium oscillations have been reported over a wide range of frequencies with a chaotic or regular pattern (18).

In many biological systems, cells display spontaneous calcium oscillations (CaOs) and repetitive action-potential firing. These phenomena have been described separately by models for intracellular inositol trisphosphate (IP_3)-mediated CaOs (19, 20) and for plasma

membrane excitability (21). We have recently presented a single-cell model that combines an excitable membrane with an IP_3 -mediated intracellular calcium oscillator (22). The IP_3 -receptor is described as an endoplasmic reticulum (ER) calcium channel with open and close probabilities that depend on the cytoplasmic concentrations of calcium ($[Ca_{cyt}^{2+}]$) and IP_3 ($[IP_3]$). An essential component of this model relates to store-operated calcium channels in the plasma membrane. Since it is not known whether multiple types of store-operated calcium channels are involved in normal rat kidney (NRK) fibroblasts, we will use the general terminology of store-dependent calcium (SDC) channels.

NRK fibroblasts in cell culture exhibit growth-state dependent changes in their electrophysiological behavior (23). Subconfluent-grown serum-deprived quiescent cells exhibit a stable resting membrane potential near -70 mV ("resting state"). Upon subsequent treatment with epidermal growth factor the cells re-enter the cell cycle, undergo density-dependent growth-arrest (contact inhibition) at confluence and spontaneously fire action potentials associated with intracellular calcium oscillations ("AP-firing state"). Subsequent addition of retinoic acid or transforming growth factor (TGF) β to the contact inhibited cells causes the cells to become phenotypically transformed and to depolarize the cell to approximately -20 mV ("depolarized state"). This depolarization has been shown to be caused by an elevation of the concentration of prostaglandin (PG) $F_{2\alpha}$ secreted by the unrestricted proliferating transformed cells. Washout of the medium conditioned by the transformed cells by perfusion with fresh serum-free medium causes the cells to slowly repolarize, and, preceded by a short period of fast small-amplitude spiking of their membrane potential ("fast oscillating state"), to regain spontaneous repetitive action potential firing activity ("AP-firing state") similar to that of the contact inhibited cells. These phenomena have been described in detail (23) and are very similar to the behavior of other cell types with calcium oscillations and action potential firing, such as interstitial cells of Cajal (24) and hepatocytes (25).

In this study we have analyzed the model reported in (22). This model, which is shown schematically in Fig. 1, illustrates the basic characteristics of NRK fibroblasts. It repro-

duces, on the basis of single-cell data (22, 26), the dynamics of both the plasma membrane excitability and that of the intracellular calcium oscillator. We have recently shown that $(PG)F_{2\alpha}$ dose-dependently induces IP_3 -dependent intracellular calcium oscillations in NRK fibroblasts (27). Since the growth-state dependent modulation of the membrane potential of NRK fibroblasts is related to the concentration of $(PG)F_{2\alpha}$ in their culture medium (23) and since this prostaglandin dose-dependently increases $[IP_3]$, we took $[IP_3]$ as a control parameter to analyze the stability of the single-cell model.

The stability analysis shows how coupling of an excitable membrane with an intracellular calcium oscillator leads to a rich behavior of a cell with multiple stable and unstable states with hysteresis. We show that the growth-state dependent modulations of the membrane potential of NRK fibroblasts in cell culture described above can be understood as the stable states of the single-cell model with membrane excitability and calcium oscillations of these cells. The stable states of the model reproduce the four growth-dependent states of NRK cells, corresponding to the resting state at -70 mV, the AP-firing state for spontaneous action potential firing, the depolarized state at -20 mV and the fast oscillating state with small-amplitude spiking around -20 mV. Therefore, the four growth-dependent states of NRK fibroblasts may not reflect the behavior of cells that have differentiated into different cell types with different properties, but reflect four different states of a single cell type, that is characterized by a single model.

Model description

The dynamics of NRK cell membrane excitability is given by a set of equations which describe the active and passive ion transport systems in the plasma membrane and the endoplasmic reticulum, as illustrated in Fig. 1 (see (21, 22) for a detailed description). The change in the membrane potential as a function of time due to the currents through inwardly rectifying potassium channels (I_{Kir}), L-type Ca-channels (I_{CaL}), Ca-dependent Cl-channels ($I_{Cl(Ca)}$),

leak channels (I_{lk}), and SDC-channels (I_{SDC}) is given by

$$C_m \frac{dV_m}{dt} = -(I_{Kir} + I_{lk} + I_{CaL} + I_{Cl(Ca)} + I_{SDC}). \quad (1)$$

I_{Kir} and I_{lk} determine the membrane potential of the cell at rest near -70 mV and are specified in (22).

The equation describing the L-type Ca-current (I_{CaL}) in terms of the Hodgkin-Huxley kinetics of the L-type Ca-channel, is given by

$$I_{CaL} = m \ h \ v_{Ca} \ G_{CaL} (V_m - E_{CaL}), \quad (2)$$

where m is the voltage-dependent activation variable, h is the voltage-dependent inactivation variable and v_{Ca} is the inactivation parameter. The dynamics of the variables m and h are described by first order differential equations of the Hodgkin-Huxley type (22). The calcium-dependent inactivation is given by $v_{Ca} = K_{vCa}/([Ca_{cyt}^{2+}] + K_{vCa})$.

The Ca-dependent Cl-current $I_{Cl(Ca)}$ is given by

$$I_{Cl(Ca)} = \frac{[Ca_{cyt}^{2+}]}{[Ca_{cyt}^{2+}] + K_{Cl(Ca)}} G_{Cl(Ca)} (V_m - E_{Cl(Ca)}) \quad (3)$$

The chloride current increases with the cytosolic calcium concentration $[Ca_{cyt}^{2+}]$, causing a depolarization to the Nernst potential of chloride ions ($E_{Cl(Ca)}$) near -20 mV in NRK fibroblasts for sufficiently high values of $[Ca_{cyt}^{2+}]$.

The store-dependent calcium current I_{SDC} is described by

$$I_{SDC} = \frac{K_{SDC}}{[Ca_{ER}^{2+}] + K_{SDC}} G_{SDC} (V_m - E_{SDC}). \quad (4)$$

This store-dependent calcium channel allows calcium ions to flow from the extracellular space into the cytosol at a rate inversely proportional to the calcium concentration in the ER (28).

SDC channels are thought to play a major role in the control of Ca-homeostasis in the cell (22, 29).

The rate of change of Ca-content of the cytosol of the cell due to inflow through the cell membrane and from the ER store, and by buffering is described by

$$Vol_{cyt} \frac{d[Ca_{cyt}^{2+}]}{dt} = A_{PM} J_{PM} + A_{ER} (J_{IP_3R} + J_{lkER} - J_{SERCA}) - Vol_{cyt} \frac{d[BCa]}{dt}, \quad (5)$$

where Vol_{cyt} represents the cytoplasmic volume and A_{PM} and A_{ER} the area of the cell membrane and of the ER membrane, respectively. The term $[BCa]$ denotes the buffer-calcium complex in the cytosol and will be explained later. The flux of calcium through the membrane (J_{PM}) is the sum of the influxes of Ca^{2+} ions through the L-type Ca-channel, through the SDC-channel, and of the extrusion by the PMCA-pump (22), and is given by $J_{PM} = -(1/(z_{Ca} F A_{PM}))(I_{CaL} + I_{SDC}) - J_{PMCA}$.

The dynamics for the intracellular calcium oscillator is described by the flux of calcium through the ER membrane. The rate of change of calcium content in the ER depends on the sum of flux through the IP₃-receptor (J_{IP_3R}), flux by leak through the ER-membrane (J_{lkER}) and flux by removal by the SERCA pump (J_{SERCA}), which results in

$$Vol_{ER} \frac{d[Ca_{ER}^{2+}]}{dt} = A_{ER} (-J_{IP_3R} - J_{lkER} + J_{SERCA}), \quad (6)$$

where Vol_{ER} represents the volume of the ER.

The flux through the IP₃-receptor is described by

$$J_{IP_3R} = f_{\infty}^3 w^3 K_{IP_3R} ([Ca_{ER}^{2+}] - [Ca_{cyt}^{2+}]) \quad (7)$$

where $[Ca_{ER}^{2+}] - [Ca_{cyt}^{2+}]$ is the concentration difference between calcium in the ER and in the cytosol. K_{IP_3R} is the rate constant per unit area of IP₃-receptor mediated release. The terms

f_∞ and w represent the fraction of open activation and inactivation gates, respectively. f_∞ and w_∞ depend both on the cytosolic calcium concentration and are described by

$$f_\infty = \frac{[Ca_{cyt}^{2+}]}{K_{fIP_3} + [Ca_{cyt}^{2+}]} \quad (8)$$

and

$$w_\infty = \frac{\frac{[IP_3]}{K_{wIP_3} + [IP_3]}}{\frac{[IP_3]}{K_{wIP_3} + [IP_3]} + K_{w(Ca)}[Ca_{cyt}^{2+}]} \quad (9)$$

The inactivation time constant of the IP_3 -receptor is defined by

$$\tau_w = \frac{a}{\frac{[IP_3]}{K_{wIP_3} + [IP_3]} + K_{w(Ca)}[Ca_{cyt}^{2+}]} \quad (10)$$

K_{fIP_3} , K_{wIP_3} , $K_{w(Ca)}$ and a are constants. The fraction of open activation gates (f) is independent of the IP_3 concentration, but increases when the calcium concentration in the cytosol increases. The fraction of open inactivation gates (w) depends on the IP_3 concentration and on $[Ca_{cyt}^{2+}]$. τ_w determines the duration of the de-inactivation of w.

J_{lkER} is a passive leak of Ca^{2+} from the ER into the cytosol which is not mediated by the IP_3 -receptor, but by an additional Ca-channel in the ER membrane, presumably the translocon. Experimental evidence for a role of the translocon complex as a passive Ca^{2+} leak channel has been presented recently (30). J_{lkER} is given by $J_{lkER} = K_{lkER}([Ca_{ER}^{2+}] - [Ca_{cyt}^{2+}])$. We used the leakage parameter K_{lkER} as a control parameter to study the dynamics of the plasma membrane, because changes in the leak of Ca-ions through the ER membrane produce proportional changes in $[Ca_{cyt}^{2+}]$.

J_{SERCA} represents the flux of calcium into the ER by the SERCA pump and is given by $J_{SERCA} = J_{SERCA}^{max} \{[Ca_{cyt}^{2+}]^2 / (K_{SERCA}^2 + [Ca_{cyt}^{2+}]^2)\}$.

Finally, calcium in the cytosol is buffered by proteins in the cytosol. The dynamics of buffering is given by $d[BCa]/dt = k_{on}([T_B] - [BCa])[Ca_{cyt}^{2+}] - k_{off}[BCa]$, where $[T_B]$ is the

total concentration of buffer in the cytosol and k_{on} and k_{off} are the buffer rates (22).

The excitable membrane and the IP_3 -mediated intracellular calcium oscillator are coupled by the Ca-concentration $[Ca_{cyt}^{2+}]$ in the cytosol as explained in (22). During an action potential, opening of the L-type Ca-channel causes a large inward current of Ca-ions through the plasma membrane. The increased $[Ca_{cyt}^{2+}]$ activates the IP_3 -receptor (calcium release channel), causing calcium release from the ER, which further contributes to the intracellular cytosolic calcium transient. In the reverse process, IP_3 -mediated calcium oscillations cause periodic calcium transients, which lead to periodic opening of the Ca-dependent Cl-channels. The depolarization of the membrane potential towards the Nernst potential of the Ca-dependent Cl-channels near -20 mV causes activation of the L-type Ca-channels in the plasma membrane and excitation (21, 31). After an action potential or Ca-transient the reduction of cytosolic calcium by the activity of the SERCA and PMCA pumps reduces $I_{Cl(Ca)}$ (see Eq. 3), enough to allow the membrane to return to the membrane potential at rest near -70 mV.

The dynamics of the single-cell model depends on seven variables (m , h , w , $[BCa]$, V_m , $[Ca_{cyt}^{2+}]$ and $[Ca_{ER}^{2+}]$), which were defined above. To study the stability of the complete system we have determined the singular states for the system and calculated the Floquet multipliers of these singular states (32, 33).

Stability analysis of the membrane model

We will first analyze the bifurcations and local stability of both the excitable membrane and intracellular calcium oscillator separately, and then compare the results with the properties of the single-cell model including both the membrane dynamics and intracellular calcium oscillator. Two different analyses, namely, our own implementation in C , and the software package $XPPAUT$ (34), which includes an $AUTO86$ (35) interface, gave the same results.

In the single-cell model the intracellular calcium oscillations can be eliminated by setting the IP_3 concentration ($[IP_3]$) to zero. This allows the study of the excitable cell membrane

separately from the calcium oscillator. The dynamics of the plasma membrane depends on the cytosolic calcium concentration $[Ca_{cyt}^{2+}]$, which opens the Ca-dependent Cl-channel. Since the leak of Ca-ions from the ER affects the mean value of $[Ca_{cyt}^{2+}]$, the dynamics of the membrane is studied as a function of the leakage parameter K_{lkER} . Fig. 2 shows a hysteresis diagram for the excitable cell membrane with the steady states of the calcium concentration in the cytosol ($[Ca_{cyt}^{2+}]$, panel A) and of the membrane potential (V_m , panel B). The thick and thin solid lines refer to the stable states for increasing and decreasing values of K_{lkER} , respectively. The dashed-dotted lines reflect the transitions between the two stable branches for increasing and decreasing values of K_{lkER} .

Starting at the value zero for K_{lkER} , the inwardly rectifying K-channels keep the membrane potential at the resting membrane potential of the NRK fibroblasts near -70 mV, where the membrane is able to produce an action potential upon electrical stimulation (22). For increasing values of K_{lkER} , $[Ca_{cyt}^{2+}]$ and V_m increase gradually, causing a decreasing threshold for activation. The gradual increase of V_m is due to gradual opening of the Ca-dependent Cl-channels for increasing $[Ca_{cyt}^{2+}]$ (see Eq. 3). At $K_{lkER} \approx 58.0 \times 10^{-8} \text{ dm/s}$, $[Ca_{cyt}^{2+}]$ is large enough to open the Ca-dependent Cl-channels driving the membrane potential towards the Nernst potential for Cl^- -ions which is near -20 mV in NRK fibroblasts (see Fig. 2B). The resulting depolarization causes closure of the inwardly rectifying K-channels and opening of the L-type Ca-channels which leads to an increase of calcium inflow from the extracellular medium into the cytosol. The positive feedback via the membrane potential between Ca-dependent Cl-channels and L-type Ca-channels explains the abrupt increase of $[Ca_{cyt}^{2+}]$ (dashed-dotted line) to $2.3 \mu M$.

When we decrease K_{lkER} starting from $60.0 \times 10^{-8} \text{ dm/s}$ (thin solid line), the cell remains depolarized near -20 mV far below the value of K_{lkER} at $58.0 \times 10^{-8} \text{ dm/s}$. This is caused by the feedback between the Ca-dependent Cl-channels and L-type Ca-channels. When K_{lkER} decreases, $[Ca_{cyt}^{2+}]$ also decreases, which reduces the fraction of open Ca-dependent Cl-channels. As a consequence, the membrane potential slightly decreases just below -20

mV, which leads to an increased fraction of open L-type Ca-channels, since the product of m_h of steady-state activation and inactivation (see Eq. 2) reaches a maximum just below -20 mV. The increment of the fraction of open L-type Ca-channels leads to an extra inflow of calcium in the cytosol, which increases the fraction of the open Ca-dependent Cl-channels and prevents the system from falling back to a membrane potential near -70 mV. Thus, in spite of the slow decrease of calcium concentration and membrane potential caused by the leak channels, the feedback by the L-type Ca-channels keeps the system at an elevated $[Ca_{cyt}^{2+}]$ and membrane potential near -20 mV until low values K_{lkER} . The calcium in the cytosol returns to a low concentration, only when the K_{lkER} is decreased to very low values. Then the Ca-dependent Cl-channels close and the membrane potential repolarizes to -70 mV. Separate simulations showed that the inward rectifier contributes to the transitions, but not to the hysteresis.

Stability analysis of the intracellular calcium oscillator

Following a similar plan as for the excitable cell membrane, we obtained a bifurcation diagram for the intracellular calcium oscillator as a function of the IP_3 concentration under conditions that the L-type Ca-channels are blocked such as with nifedipine. This was achieved by setting G_{CaL} to zero and K_{lkER} to its physiological value of $2.0 \times 10^{-8} \text{ dm/s}$. In this way, we eliminate the contribution of calcium inflow by the L-type Ca-channels and remove a principal influence of the membrane model on the intracellular calcium oscillator. Therefore, we only take into account the Ca-flux through the SDC-channels and PMCA pump in the plasma membrane.

As explained in (22), the relative strength of the PMCA and SERCA pump is crucial to reproduce the steady state calcium concentrations in the cytosol and in the ER. By eliminating the calcium inflow by the L-type Ca-channels, less calcium flows into the cell. Therefore, we have to change the relative strength of the PMCA and/or SERCA pump to maintain the proper balance between calcium concentration in the cytosol and ER. In this

model study, we choose to decrease the strength of the SERCA pump. By doing so, the system reveals a bifurcation diagram (Fig. 3A) similar to that observed in other models (36, 37).

Fig. 3A shows the dynamical behavior of $[Ca_{cyt}^{2+}]$ as a function of $[IP_3]$ for $G_{CaL} = 0$ and with J_{SERCA}^{max} set to $2 \times 10^{-5} \text{ } (\mu\text{mol})/(s \times dm^2)$. Fig. 3A shows a single stable steady state for small values of $[IP_3]$ (range $0.0 - 0.2 \mu\text{M}$). At $[IP_3]$ near $0.2 \mu\text{M}$ the dynamics reveals a supercritical Hopf bifurcation (thick solid line), and the system becomes a calcium oscillator in the range of IP_3 concentrations between 0.2 and $3.6 \mu\text{M}$. For $[IP_3]$ values near $3.6 \mu\text{M}$ the system meets a supercritical Hopf bifurcation and remains stable for higher IP_3 concentration at a Ca-concentration near $5 \mu\text{M}$. In the range for $[IP_3]$ above $3.5 \mu\text{M}$, the elevated mean level of $[Ca_{cyt}^{2+}]$ gives rise to a short time constant τ_w for the inactivation parameter w (Eq. 10). Due to this small time constant the inactivation w recovers relatively fast compared to the removal of $[Ca_{cyt}^{2+}]$, i.e. before the activation parameter f de-activates to small values. As a result the product fw does not reach small values and the IP_3 -receptor remains open (see Eq. 7), causing a constant leak of calcium.

For decreasing $[IP_3]$ values (thin solid line), the system starts at a stable fixed point which remains stable until $3.50 \mu\text{M}$. In the range $[IP_3]$ between 3.5 and $3.6 \mu\text{M}$, the system exhibits bistability and a hysteresis over a small range of IP_3 -values. This hysteresis is caused by the positive feedback between $[Ca_{cyt}^{2+}]$ and the activation gate (f). For decreasing $[IP_3]$, the $[Ca_{cyt}^{2+}]$ is already elevated and so a large fraction of activation gates f is already open and the time constant τ_w is short. Due to the short time constant τ_w , the time for de-inactivation (w) is faster than for de-activation (f). As a consequence, the product of f and w does not reach small values and calcium passes continuously through the IP_3 -receptor from the store into the cytosol. This hysteresis did not show up in the figures presented by Li & Rinzel (36), but appears in their model if we insert the parameter values which apply to the NRK fibroblasts (see (22)).

For $[IP_3]$ values below $3.5 \mu\text{M}$, the stable fixed point disappears, and the system starts

to operate as an oscillator, until $[IP_3]$ values smaller than $0.15 \mu M$, where the system returns to a single stable steady state.

As a next step, we have set the strength of the SERCA pump back to its default value $8.10^{-5} \mu mol/(s \times dm^2)$ which corresponds to the value in the single-cell model with an excitable membrane and IP_3 -mediated calcium oscillations. This results in the bifurcation diagram shown in Fig. 3B. Fig. 3B shows a major hysteresis in the $[IP_3]$ range between 8 and $53 \mu M$ (see inset). To compare the results with those in Fig. 3A we scaled Fig. 3B in the same $[IP_3]$ range as in Fig. 3A.

When the strength of the SERCA pump is increased to $8.10^{-5} \mu mol/(s \times dm^2)$, $[Ca_{cyt}^{2+}]$ decreases more rapidly after a calcium transient. This affects the time constant τ_w of the inactivation parameter w (see Eq. 10). For small $[Ca_{cyt}^{2+}]$ levels, this time constant is relatively large, ensuring a slow de-inactivation. This explains why a more powerful SERCA pump gives rise to calcium oscillations over a much larger range of IP_3 concentrations. Only at sufficiently large $[IP_3]$ values does τ_w become sufficiently small such that de-inactivation (w) takes place more rapidly than de-activation (f). For these high IP_3 -values, the product fw of the activation parameter (f) and the inactivation parameter (w) is large enough to allow a continuous leak of calcium through the IP_3 -receptor.

The inset in Fig. 3B shows a single stable steady state for small values of $[IP_3]$. At $[IP_3]$ near $0.2 \mu M$, the dynamics reveals a subcritical Hopf bifurcation (thick solid line), and the system becomes a calcium oscillator in the range of IP_3 concentrations between 0.2 and $53 \mu M$. For $[IP_3]$ above $53 \mu M$, $[Ca_{cyt}^{2+}]$ is elevated at a steady state concentration near $4 \mu M$. For decreasing $[IP_3]$ values (thin solid line), the system starts at a stable elevated $[Ca_{cyt}^{2+}]$ which remains stable until $[IP_3]$ is near $8 \mu M$. For $[IP_3]$ values below $8 \mu M$, the stable fixed point disappears, and the system starts to operate as an oscillator, until $[IP_3]$ values smaller than $0.2 \mu M$. We conclude that increasing the activity of the SERCA pump makes it more easy for the cell to oscillate at higher $[IP_3]$ values and causes a hysteresis over a larger range of $[IP_3]$ values.

Stability analysis of the single-cell model

Unblocking the L-type Ca-channels ($G_{CaL} = 0.7 \mu M$) transforms the bifurcation diagram of 3B into that of Fig. 4A. Fig. 4 shows $[Ca_{cyt}^{2+}]$ (panel *A*) and the membrane potential (panel *B*) as a function of IP_3 concentration in the cell. The solid and dashed-dotted lines represent stable and unstable states, respectively. For small $[IP_3]$ values in the range from 0.00 to 0.15 μM , the cell has a single stable steady state ("resting state") with a membrane potential near -70 mV. For $[IP_3] > 0.15 \mu M$, the stable fixed point becomes unstable in a subcritical Hopf bifurcation. Calcium oscillations together with action potentials occur for IP_3 concentrations in the range between 0.15 and $1.75 \mu M$ ("AP-firing state") (see panel *C* which shows the membrane potential as a function of time for $[IP_3] = 0.7 \mu M$). In this regime, a rapid calcium inflow from the *ER* into the cytosol opens the Ca-dependent Cl-channel, causing an inward current towards the Cl-Nernst potential close to -20 mV. This depolarization activates the L-type Ca-channels leading to an AP. After closure of the IP_3 -receptor, calcium is removed from the cytosol by the Ca-pumps in the cell membrane and ER, leading to repolarization to -70 mV. For $[IP_3] > 1.75 \mu M$, the fixed point ($[Ca_{cyt}^{2+}], V_m$) near $(3.00 \mu M, -20$ mV) becomes stable in a subcritical Hopf bifurcation ("depolarized state"). This can be understood from the fact that the time-constant τ_w (see Eq. 10) for calcium-dependent (de-)inactivation of the IP_3 -receptor decreases for increasing values of $[IP_3]$ and for increasing values of the mean $[Ca_{cyt}^{2+}]$. Near $[IP_3] = 1.75$, the time-constant τ_w is relatively short. During a cytosolic calcium transient the fast inactivation of the inactivation gates w of the IP_3 -receptor is followed by a fast de-inactivation of the inactivation gates of the IP_3 -receptor. During the fast de-inactivation, the fraction of open activation gates f of the IP_3 -receptor is still high due to high $[Ca_{cyt}^{2+}]$ (because removal of calcium through the SERCA and PMCA pump is not fast enough). As a consequence the IP_3 -receptor remains open. Now the IP_3 -receptor acts as a constant leak channel, like J_{lkER} . This leak of calcium into the cytosol opens the Ca-dependent Cl-channels, causing a maintained depolarization to the Cl-Nernst potential near -20 mV ("depolarized state") (panel *B*).

If $[IP_3]$ is decreased starting from $[IP_3] = 2.5 \mu M$, the cell with both the excitable membrane and intracellular calcium oscillator active exhibits a complex hysteresis pattern. For decreasing IP_3 concentrations, the system stays in a single stable state (solid line) at an elevated $[Ca_{cyt}^{2+}]$ near $3 \mu M$ and a membrane potential near $-20 mV$ until $[IP_3] \approx 0.85 \mu M$ ("depolarized state"). Then, the cell goes through a Hopf bifurcation (dashed line) forcing the system to behave as a stable oscillator with small calcium oscillations with an amplitude of about $6 \mu M$ and with small membrane potential oscillations around $-23 mV$ ("fast oscillating state"). These small oscillations of the membrane potential just below $-20 mV$ are illustrated in more detail in panel D. Note that the oscillations of the membrane potential in panels C and D are both obtained for $[IP_3] = 0.7 \mu M$, illustrating the hysteresis. The oscillations shown in panel D are due to small IP_3 -mediated calcium oscillations with active involvement of the L-type Ca-channel dynamics. Due to decreasing $[IP_3]$, the de-inactivation time constant τ_w of the IP_3 -receptor increases gradually. This makes it possible for the cell to generate calcium oscillations. Setting v_{ca} in the equation for the L-type Ca-current to 1 does not change the bifurcation diagram of Fig. 4. The shape of the bifurcation scheme in Fig. 4A remains the same, but the calcium oscillations extend over a larger range of $[Ca_{cyt}^{2+}]$ -values (approximately twice as large).

At $[IP_3] \approx 0.45 \mu M$ the stable small-amplitude oscillator becomes unstable (dashed line), returning the system to the stable oscillations with large amplitude Ca-oscillations with a peak value near $20 \mu M$ and with action potentials in the range between -70 and $-10 mV$ ("AP-firing state"). Finally, for $[IP_3]$ values smaller than $0.15 \mu M$ the system returns to a single stable state ("resting state").

In comparison with the simple dynamics of the cell membrane and intracellular Ca-oscillator, shown in Figs. 2 and 3, it is remarkable to see the complex behavior of the single-cell model shown in Fig. 4.

Since the SDC channels in the plasma membrane play a crucial role in stabilization of the calcium dynamics (22, 38), we studied the dynamics of the cell as a function of the SDC

conductance in a range between 0.00 and 0.20 nS. Fig. 5 shows the hysteresis diagrams for five different values of G_{SDC} . As explained in (22), the calcium homeostasis of the cell is unstable for $G_{SDC} = 0.00$ nS. For small values of G_{SDC} bistability and hysteresis appears. The IP_3 range with hysteresis is largest for a G_{SDC} value near 0.04 nS (see Fig. 5). For higher values of G_{SDC} , the range of hysteresis decreases until the typical Hopf-bifurcation for the intracellular IP_3 -mediated calcium oscillations remains for $G_{SDC} = 0.20$ nS.

The IP_3 range of the hysteresis as a function on the SDC conductance channel is shown in Fig. 6. We define the IP_3 range of hysteresis as the range of $[IP_3]$ in which multiple states are found for increasing and decreasing $[IP_3]$. For example, in Fig. 4 hysteresis takes place for $[IP_3]$ values between 0.45 and 1.75 μM , giving an IP_3 range of hysteresis of 1.3 μM .

Recent data in the literature show that the SDC conductance, which was found to give the largest range for hysteresis in our study (near 0.04 nS), corresponds to the observed SDC conductance in other studies (39, 40, 41). The SDC conductance reported in Table 1 of (39) and in (40) was in the range between 0.04 and 0.05 nS (solid line below the peak in Fig. 6). For hepatocytes (41) a SDC conductance was reported in the range between 0.08 and 0.14 nS. However, since the density of all ion channels in hepatocytes is twice as high as in fibroblast (42, 43), the ratio of conductances for the ion channels is the same in hepatocytes and NRK fibroblasts. If we correct for this higher density, rescaling all conductances for those of NRK fibroblasts, we obtain the dotted line in 6. Therefore, the SDC conductance, for which hysteresis is found over the largest range of IP_3 - values in our study (see Figs. 5 and 6), is in agreement with experimental observations for SDC conductance.

Discussion

In this study we have analyzed a relatively simple model with an excitable membrane and with IP_3 -mediated calcium oscillations. The interaction between these mechanisms in a single-cell model revealed a surprisingly rich behavior with stable/instable states with hysteresis.

The hysteresis and bistability of the membrane potential and the intracellular calcium concentration in Fig. 4A and B obtained by stability analysis of the single-cell model provide an explanation for the various growth-state dependent changes in the electrophysiological behavior of normal rat kidney (NRK) fibroblasts in cell culture (23). The stability analysis of the single-cell model (Fig. 4) reveals for low $[IP_3]$ values (range 0.0 - 0.2 μM) a cell in the "resting state". Increasing the $[IP_3]$ leads to spontaneous AP firing ("AP-firing state") and at high $[IP_3]$ values above 1.75 μM , the cell depolarizes ("depolarized state"). When we start at an $[IP_3]$ value of 2.0 μM and decrease $[IP_3]$, the system is in the "depolarized state" and changes from the "fast oscillating state" (range 0.45 - 0.8 μM) to the "AP-firing state" (range 0.2 - 0.45 μM) back to its "resting state" (range 0.0 - 0.2 μM), which is in agreement with experimental data shown by Harks et al. (27). In the study of Harks et al. (23) washout of the medium conditioned by the transformed cells by perfusion with fresh serum-free medium, causes the cells to slowly repolarize, and, preceded by a short period of fast small-amplitude spiking of their membrane potential ("fast oscillating state"), to regain spontaneous repetitive action potential firing activity similar to that of the contact inhibited cells. This compares well with the results in Fig. 4B, which shows for decreasing $[IP_3]$ a very similar behavior. Therefore, we conclude that the stable states of the model as revealed by stability analysis of the single-cell model correspond in great detail to the observed growth-state dependent modulations of the membrane potential of NRK fibroblasts in cell culture. This strongly suggests that these growth-state dependent modulations of the membrane potential of NRK cells reflect just different states of the same cell, rather than the behavior of cells, that have differentiated to different cell types with different properties during the various stages of growth-factor stimulated development in vitro.

Most of the parameter values in our model were taken from the literature (see (22)) for a detailed overview). Interestingly, the parameter values for the excitable membrane and for the IP_3 -mediated calcium oscillator, which are very different mechanisms, are not independent. This can be understood from the fact that the dynamics of the excitable membrane

and of the IP_3 receptor are coupled by the cytosolic calcium concentration. Changing one parameter of the excitable membrane or calcium oscillator affects the other mechanism by changes in the cytosolic calcium concentration. This is illustrated, for example, by Fig. 3. Changing the strength of the SERCA pump causes large differences in the range of hysteresis in the dynamics of cytosolic calcium (Fig. 3), and therefore also in the dynamics of the membrane potential (see Fig. 4, which illustrates the relation between the dynamics of cytosolic calcium and the membrane potential). Although the parameter values for the excitable membrane and for the IP_3 -mediated calcium oscillator were taken from different studies, they fit nicely together to explain the behavior of NRK cells both qualitatively and quantitatively. This provides strong evidence for the reliability of these parameter values. Moreover, this suggests that cells should have complicated regulatory mechanisms to control all parameter values within a proper range of parameter values to ensure the proper cell dynamics.

Summarizing, we explored the dynamical properties of a single-cell model reproducing experimental observations on calcium oscillations and action potential generation in NRK fibroblasts. A bifurcation analysis revealed hysteresis and a complex spectrum of stable and unstable states, which allows the system to switch among different stable branches. Stability of the cell behavior is dominated by the homeostatic function of the SDC channel. The conductance, which provides the largest IP_3 range for hysteresis, compares well with experimental values for this conductance (39, 40, 41). Experimental observations in NRK fibroblasts revealed the same kind of hysteresis as shown by this study.

We acknowledge financial support from the Nederlandse Organisatie voor Wetenschappelijk Onderzoek (NWO), Ministerio de Educacion y Ciencia (MEC), Junta de Andalucia (JA) and Engineering and Physical Sciences Research Council (EPSRC), projects NWO 805.47.066, MEC FIS2005-00791, JA FQM-165 and EPSRC EP/C0 10841/1.

References

- [1] Murray, J. D. (2002) *Mathematical Biology I. An Introducion*. (Springer, New York).
- [2] Keener, J. & Sneyd, J. (1998) *Mathematical Physiology*. (Springer, New York).
- [3] Haken, H. (1975) *Rev Mod Phys* **47**, 67–121.
- [4] Jones, B. J. T. (1976) *Rev Mod Phys* **48**, 107–149.
- [5] Normand, C., Pomeau, Y. & Velarde, M. G. (1977) *Rev Mod Phys* **49**, 581–624.
- [6] Cross, M. C. & Hohenberg, P. C. (1993) *Rev Mod Phys* **65**, 851–1112.
- [7] Ashwin, P. & Timme, M. (2005) *Nature* **436**, 36–37.
- [8] Rabinovich, M., Volkovskii, A., Lecanda, P., Huerta, R., Abarbanel, H. D. & Laurent, G. (2001) *Phys Rev Lett* **87**, 68–102.
- [9] Laurent, G., Friedrich, M. Stopfer R. W., Rabinovich, M. I., Volkovskii, A. & Abarbanel, H. D. (2001) *Annu Rev Neurosci* **24**, 263–297.
- [10] Pantic, L., Torres, J. J., Kappen, H. J. & Gielen, S. C. (2002) *Neural Comput* **14**, 2903–2923.
- [11] Cortes, J. M., Torres, J. J., Marro, J., Garrido, P. L. & Kappen, H. J. (2006) *Neural Comput* **18**, 614–633.
- [12] Holcman, D. & Tsodyks, M. (2006) *PLoS Comput Biol* **2**, e23.
- [13] Sha, W., Moore, J., Chen, K., Lassaletta, A. D., Yi, C. S., Tyson, J. J. & Sible, J.C. (2003) *Proc Natl Acad Sci USA* **100**, 975–980.
- [14] Solomon, M. J. (2003) *Proc Natl Acad Sci USA* **100**, 771–772.
- [15] Laurent, M. & Kellershohn, N. (1999) *Trends Biochem Sci* **24**, 418–422.

[16] Angeli, D., Ferrell, J. E. & Sontag, E. D. (2004) *Proc Natl Acad Sci USA* **101**, 1822–1827.

[17] Ferrell, J.E. (2002) *Curr Opin Cell Biol* **14**, 140–148.

[18] Chay, T. R. & Rinzel, J. (1985) *Biophys J* **47**, 357–366.

[19] De Young, G. W. & Keizer, J. (1992) *Proc Natl Acad Sci USA* **89**, 9895–9899.

[20] Sneyd, J. & Dufour, J. F. (2002) *Proc Natl Acad Sci USA* **99**, 2398–2403.

[21] Torres, J. J., Cornelisse, L. N., Harks, E. G. A., van Meerwijk, W. P. M., Theuvenet, A. P. R., & Ypey, D. L. (2004) *Am J Physiol Cell Physiol* **287**, C851–C865.

[22] Kusters, J. M. A. M., Dernison, M. M., van Meerwijk, W. P. M., Ypey, D. L., Theuvenet, A. P. R. & Gielen, C. C. A. M. (2005) *Biophys J* **89**, 3741–3756.

[23] Harks, E. G. A., Peters, P. H. J., van Dongen, J. L. J., van Zoelen, E. J. J. & Theuvenet, A. P. R. (2005) *Am J Physiol Cell Physiol* **289**, C130–C137.

[24] Ward, S.M., Ördög, T., Kohn, S.D., Abu Baker, S., Jun, J.Y., Amberg, G., Monaghan, K. & Sanders, K.M. (2000) *J. Physiol.* **525**, 355–361.

[25] Dupont, G., Koukoui, O., Clair, C., Erneux, C., Swillens, S. & Combettes, L. (2003) *FEBS Letters* **534**, 101–105.

[26] Harks, E. G., Torres, J. J., Cornelisse, L. N., Ypey, D. L. & Theuvenet, A. P. (2003) *J Cell Physiol* **196**, 493–503.

[27] Harks, E. G., Scheenen, W. J., Peters, P. H., van Zoelen, E. J. & Theuvenet, A. P. (2003) *Pflugers Arch.* **447**, 78–86.

[28] Hofer, A. M., Fasolato, C. & Pozzan, T. (1998) *J. Cell Biol.* **140**, 325–334.

[29] Feske, S., Gwack, Y., Prakriya, M., Srikanth, S., Puppel, S.H., Tanasa, B., Hogan1, P. G., Lewis, R. S., Daly, M. & Rao, A. (2006) *Nature* **441**, 179–185.

[30] Flourakis, M., Van Coppenolle, F., Lehen'kyi, V., Beck, B., Skryma, R. & Prevarskaya, N. (2006) *FASEB J.* **20**(8), 1215–17.

[31] De Roos, A.D., Van Zoelen, E. J. & Theuvenet, A. P. (1997) *J Cell Physiol* **170**, 166–173.

[32] Fairgrieve, T. F. & Jepson, A. D. (1991) *SIAM Journal on Numerical Analysis* **28**, 1446–1462.

[33] Iooss, G. & Joseph, D. (1981) *Elementary Stability and Bifurcation Theory*. (Springer, New York).

[34] Ermentrout, B. (2002) *Simulating, Analyzing, and Animating Dynamical Systems. A Guide to Xppaut for Researchers and Students*. (SIAM, Philadelphia).

[35] Doedel, E. & Kernevez, J. P. (1986) *AUTO: Software for Continuation and Bifurcation Problems in Ordinary Differential Equations*. (California Institute of Technology, Pasadena, CA).

[36] Li, Y. & Rinzel, J. (2002) *J Theor Biol* **166**, 461–473.

[37] Schuster, S., Marhl, M. & Hofer, T. (2002) *Eur J Biochem* **269**, 1333–1355.

[38] Mignen, O., Brink, C., Enfissi, A., Nadkarni, A., Shuttleworth, T. J., Giovannucci, D. R. & Capiod, T. (2005) *J Cell Sci* **170**, 166–173.

[39] Parekh, A. B. & Putney, J. W. (2005) *Physiol Rev* **85**, 757–810.

[40] Krause, E., Pfeiffer, F., Schmid, A. & Schulz, I. (1996) *J Biol Chem* **271**, 32523–32528.

[41] Rychkov, G. Y., Litjens, T., Roberts, M. L. & Barritt, G. J. (2005) *Cell Calcium* **37**, 183–191.

[42] de Roos, A. D. G. (1997) Ph.D. thesis (Katholieke Universiteit Nijmegen, The Netherlands).

[43] Yin, Z. & Watsky, M. A. (2005) *Am J Physiol Lung Cell Mol Physiol* **288**, L1110–L1116.

Figure Legends

Fig. 1.

Conceptual model of the processes involved in membrane excitability and intracellular IP_3 -mediated calcium oscillations by calcium release through IP_3 -receptors in the ER membrane in NRK fibroblasts. Cell-membrane excitability is supported by inwardly rectifying potassium channels (G_{Kir}), Ca-dependent Cl-channels ($G_{Cl(Ca)}$), L-type Ca-channels (G_{CaL}), store-dependent calcium (SDC) channels (G_{SDC}), a PMCA pump and leak channels (G_{lk}). The total flux of calcium through the ER-membrane is the result of the contribution by the SERCA pump, by the IP_3 -receptor (J_{IP_3R}) and by leak channels in the *ER* membrane (J_{lkER}). The membrane excitability and IP_3 -mediated calcium oscillations are coupled by the cytosolic calcium concentration, which is also affected by a calcium buffer B.

Fig. 2.

Stable and unstable states for the excitable membrane using K_{lkER} as a control parameter. The intracellular Ca-oscillator was silenced by setting the IP_3 concentration to zero. Thick (thin) lines correspond to the stable steady-state solutions for the $[Ca_{cyt}^{2+}]$ (panel *A*) and for the membrane potential (panel *B*) for increasing (decreasing) values of for K_{lkER} . The set of parameter values in this model was as reported in (22), with $G_{SDC} = G_{SOC}$.

Fig. 3.

The bifurcation diagram for the intracellular calcium oscillator in the single-cell model as a function of $[IP_3]$ after elimination of action potentials ($G_{CaL} = 0$) and with J_{SERCA}^{max} set to $2 \times 10^{-5} \mu mol/(s \times dm^2)$ in panel A and to $8 \times 10^{-5} \mu mol/(s \times dm^2)$ in panel B. Analogous to Fig. 2, thick and thin solid lines correspond to the stable states for increasing and decreasing values for $[IP_3]$, respectively. The three insets in panel A show the Ca-concentration as a function of time for $[IP_3]$ values at 0.01, 2 and 4 μM . The inset in B shows the stable (solid

lines) and unstable (dashed-dotted lines) states for a large range of $[IP_3]$ values. The set of all other parameter values in this model was as reported in (22), with $G_{SDC} = G_{SOC}$.

Fig. 4.

The bifurcation diagram for the single-cell model. The figure shows the stable (solid lines) and unstable (dashed-dotted lines) states for $[Ca_{cyt}^{2+}]$ (panel *A*) and the membrane potential (panel *B*) as a function of IP_3 concentration. Panel *C* and *D* show the membrane potential for $[IP_3]$ at $0.7 \mu M$ in case of increasing and decreasing $[IP_3]$, respectively. The small arrows on the curves show the direction of change of the stable modes for increasing and decreasing values of $[IP_3]$. The set of parameter values in this model was as reported in (22).

Fig. 5.

Bifurcation diagrams for the single-cell model as shown in Fig. 4A for different values of the *SDC* channel conductance from $G_{SDC} = 0.02 \text{ nS}$ (bottom) to $G_{SDC} = 0.20 \text{ nS}$ (top). At 0.04 nS (second graph from bottom), the hysteresis loop has a maximum in the $[IP_3]$ range from 0.5 to $1.95 \mu M$.

Fig. 6.

IP_3 range of the hysteresis loop in μM (cf. Fig. 5) as a function on *SDC* conductance (G_{SDC}) for a NRK cell with a capacitance of 20 pF reveals a value in which the hysteresis area is maximum (dots are simulated data). Below the peak, we illustrate the *SDC* conductance measured in experiments and separately reported in (39, 40) (solid line) and (41) (dashed line).

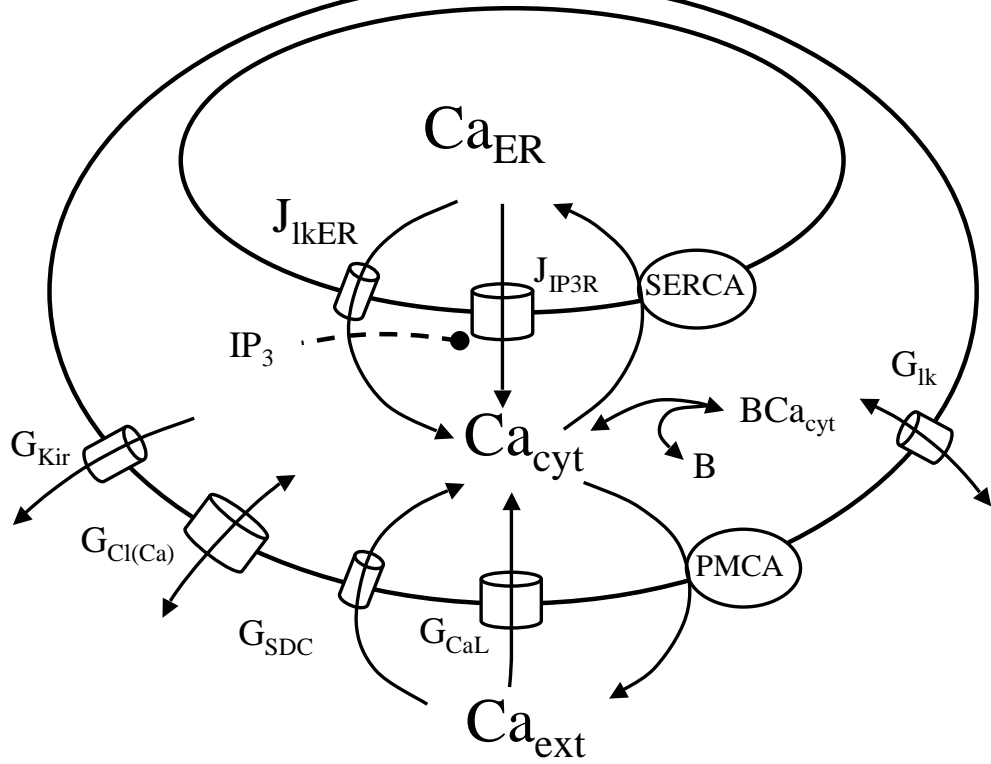


Figure 1:

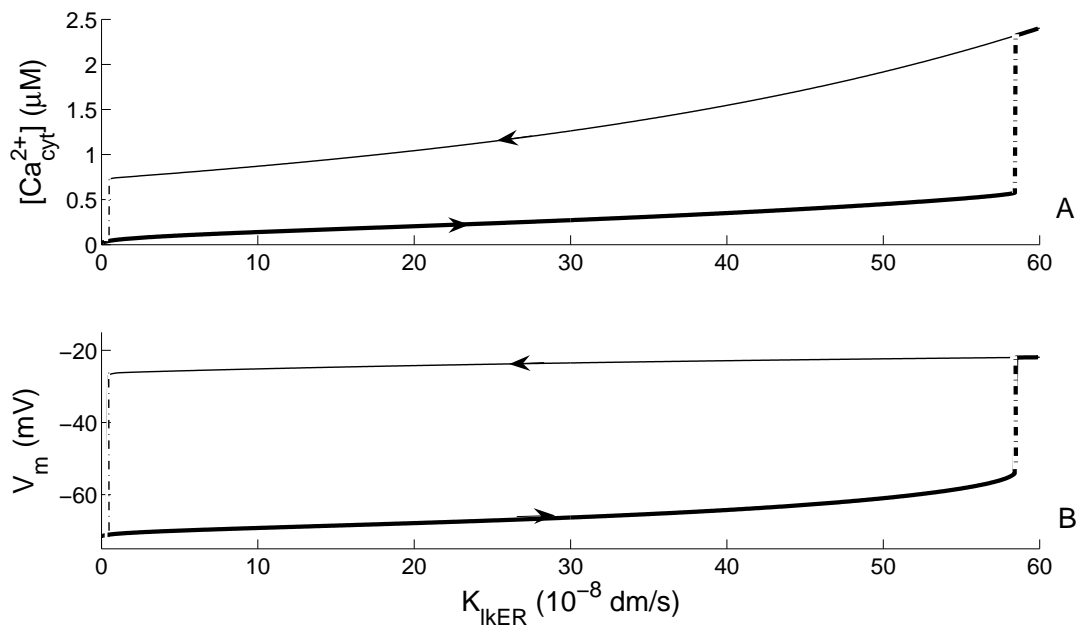


Figure 2:

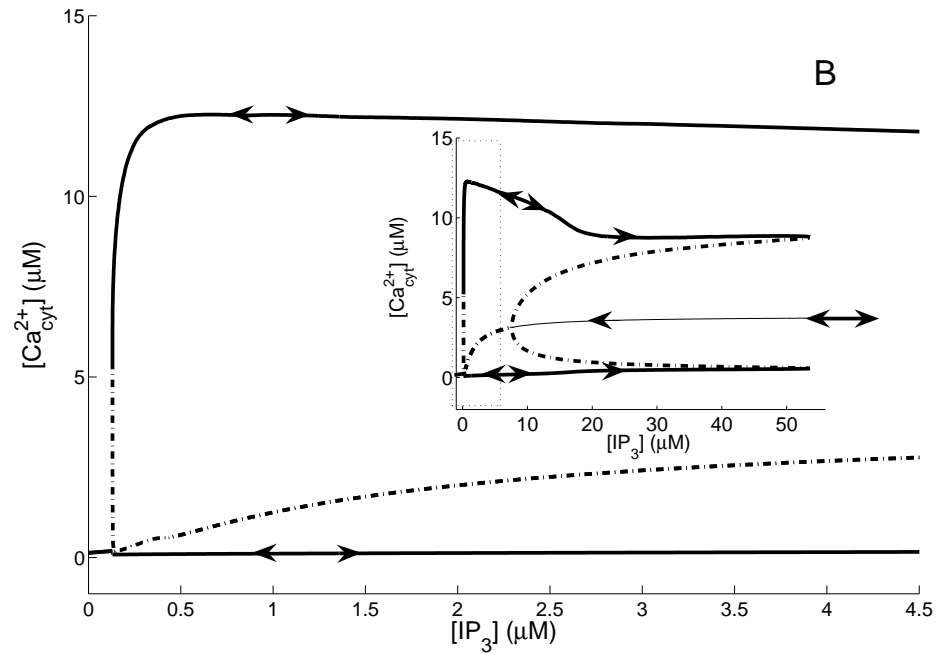
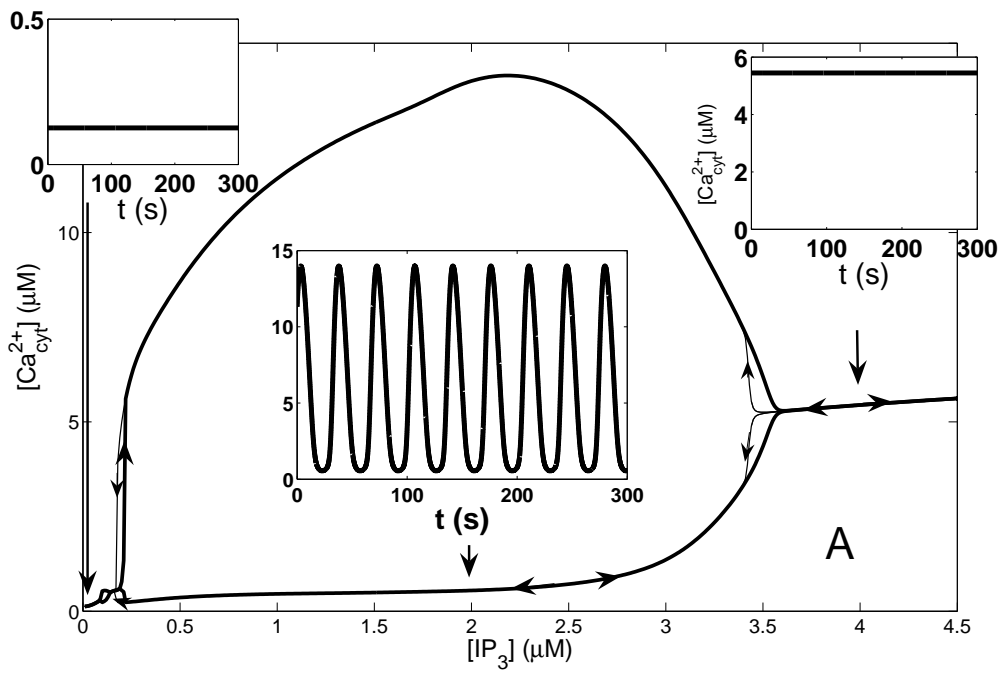


Figure 3:

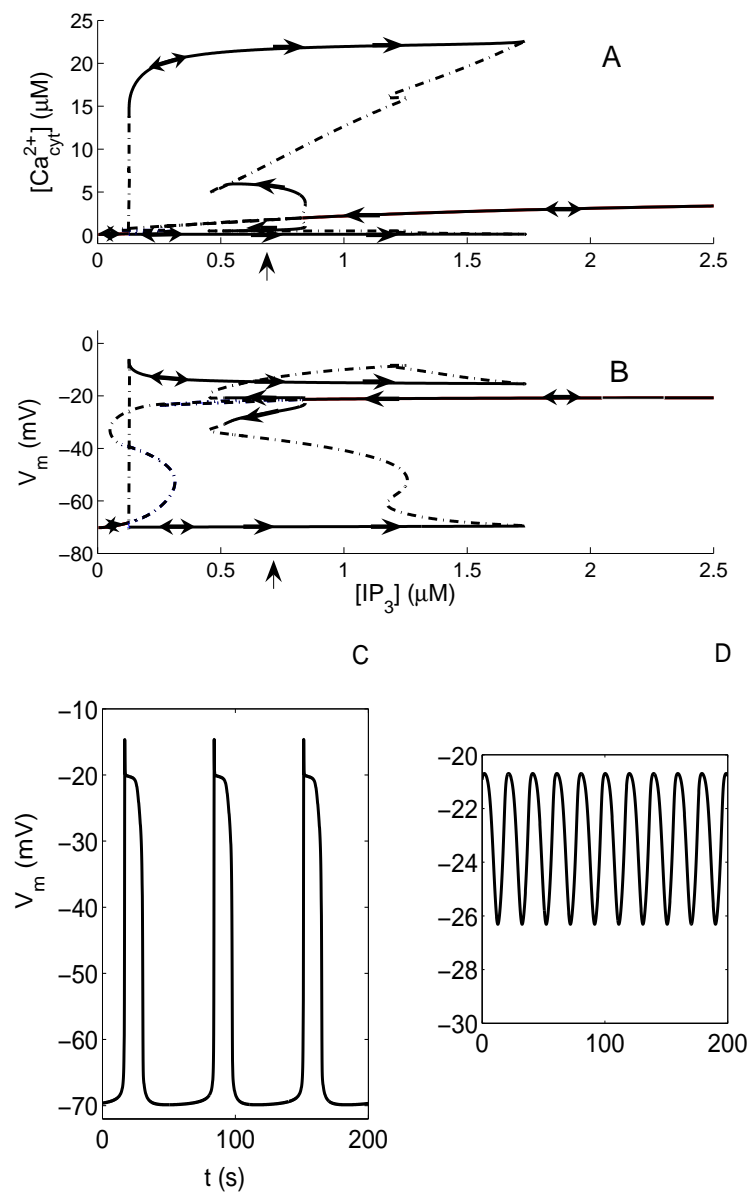


Figure 4:

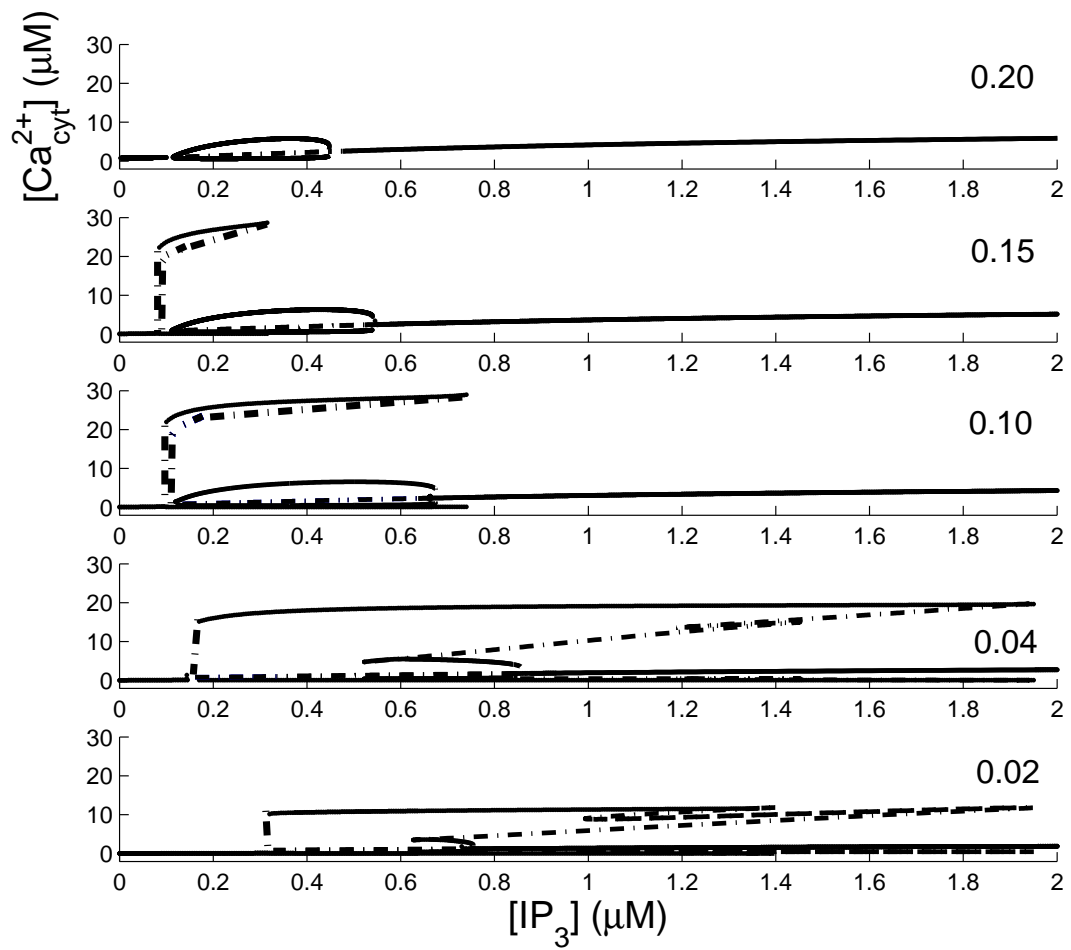


Figure 5:

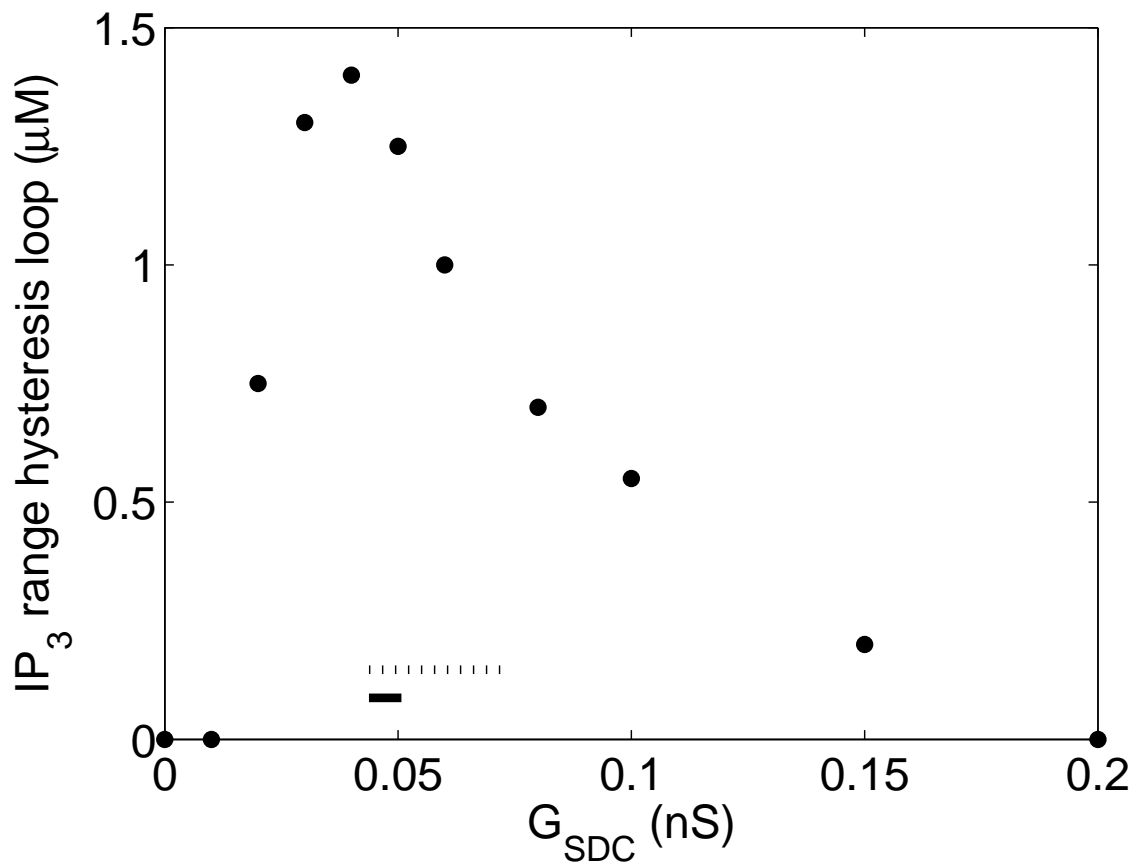


Figure 6: